Electrical Properties and Reliability of ZnO-Based Nanorod Current Emitters

I-Chuan Yao, Pang Lin, Sheng-He Huang, and Tseung-Yuen Tseng, *Fellow, IEEE*

***Abstract*— The fabrication, optical, and field emission properties of ZnO-based nanorod emitters were studied. Ga-doped ZnO nanorods combined with the formation of tip structure on top of a ZnO nanorod by oxygen plasma treatment are employed to improve the field emission properties of the nanorod emitters. By either of these two methods, the nanorod emitters exhibit significantly reduced turn-on field and enhanced field-emission factor. The morphology, crystal structure, and composition of all the nanorods used for making emitters are characterized by a scanning electron microscopy, X-ray diffraction, and energy dispersive X-ray spectrometer. The nanorods exhibit the highly preferred *c*-axis orientation single crystal structure. The photoluminescence spectra indicate the nanorods have better crystalline structure after doping and oxygen plasma treatment. Combining gallium doping process (Ga/Zn molar ratio of 1% in solution) and oxygen plasma treatment (etching time of 60 s), the tip-structured GZO nanorod emitters with tip angle of 100° have a turn-on field of 1.99 V/μm under a current density of 1 μA/cm^2, field enhancement factor of 2465, and stable operation over 2 × 10^4 s. Such improved field emission properties are attributed to decreased work function and sharp nanotips morphology. In addition, the GZO nanorod emitters with tip structure are successively and stably operated between 25 °C and 100 °C over 3000 s based on the high-temperature field emission measurement results. They have high potential for practical applications in flat panel display and light emitting device in the future.**

***Index Terms*— Field emission properties, Ga-doped ZnO nanorod emitters, oxygen plasma treatment.**

I. Introduction

ONE-DIMENSIONAL semiconductor nanostructures attract renewed interest because of their excellent optoelectronic properties and promising applications [1], [2]. Among the various applications, field emission displays had attracted a lot of interest for their high aspect ratio, proper number densities, and high emission stability [3]. Several groups have been reported on field emission from nanorods/nanowires such as carbon nanotubes [4], diamond cones [5], $Ni_{31}Si_{12}$ nanowires [6], and ZnO nanorods [7], [8]. Among 1-D nanostructure, the ZnO nanorods are considered to be one of the most promising cold cathode materials due to their large exciton binding energy, strong radiation–oxidation resistance, and high thermal stability [9], [10]. Generally, the field emission property depends on the material work function, tip morphology, and number density of nanorod emitters. But, still it is a challenge to develop the nanorod emitters having good properties and high reliability. Therefore, improvement of the field emission performances is an important issue for their application in field emission displays.

It is well known that structural properties and dopants may determine the electronic properties of the materials. The typical dopants that have been used to enhance the carrier concentrations of ZnO are the group III (Al, In, and Ga) and group IV (Sn) elements [11]–[15]. Among these elements, gallium is an effective dopant for reducing the resistivity, has less lattice distortion, and are more resistant to oxidation than aluminum. Various methods, including metal organic chemical vapor deposition and thermal evaporation [16], [17], have been reported to synthesize GZO nanorods. However, these methods required high temperature, limitation for the device applications. Therefore, we synthesize GZO nanorods by the solution method, which has the advantages of lower synthesis temperature (90 °C) and larger scale production. The effects of gallium doping on the field emission and photoluminescence (PL) properties of GZO nanorod emitters are investigated.

On the other hand, it is necessary to control the morphologies of the nanorods to improve their field emission properties because the vertically aligned ZnO nanorods have relatively large diameter and hexagonal structure at the top end. Plasma treatment is an easy and fast process to control morphology of the nanorods. We recently reported the preparation of ZnO nanotip structures from the as-grown ZnO nanorods by using the combination of chemical etching and Ar plasma treatment [18]. However, there is no literature that has ever been reported on the effect of oxygen plasma treatment on field emission properties of ZnO nanorods. In this paper, we synthesized the GZnO nanorods by using solution method and employed oxygen plasma etching method to form nanotip on the as-grown nanorods. Effects of etching time on morphology of nanostructures, and electrical and optical characteristics of ZnO nanorods are also investigated.

II. Experimental Method

P-type Si (100) substrate was cleaned by a standard Radio Corporation of America method. A thin film of zinc acetate

Manuscript received October 20, 2011; revised February 9, 2012; accepted March 19, 2012. Date of publication May 21, 2012; date of current version June 28, 2012. This work was supported by the National Science Council of ROC under Contract NSC 97-2221-E-009-150-MY3. Recommended for publication by Associate Editor B. Courtois upon evaluation of reviewers' comments.

I-C. Yao and P. Lin are with the Department of Materials Science and Engineering, National Chiao Tung University, Hsinchu 300, Taiwan (e-mail: yao.mse96g@g2.nctu.edu.tw; panglin@mail.nctu.edu.tw).

S.-H. Huang and T.-Y. Tseng are with the Department of Electronics Engineering and Institute of Electronics, National Chiao Tung University, Hsinchu 300, Taiwan (e-mail: nature75721@yahoo.com.tw; tseng@cc.nctu.edu.tw).

Color versions of one or more of the figures in this paper are available online at http://ieeexplore.ieee.org.

Digital Object Identifier 10.1109/TCPMT.2012.2194494

was spin-coated on the substrate for 10 times with a solution containing 5 mL zinc dehydrate ($C_4H_6O_4Zn{\cdot}2H_2O$, 98% purity) in ethanol. After deposition, the film was annealed at 350 °C for 30 min to produce ZnO seed layer.

GZO nanorods with different Ga/Zn molar ratios were grown by an aqueous solution method in a 70-mL solution containing 0.05 M zinc nitrate hexahydrate ($Zn(NO_3)_2{\cdot}6H_2O$, 99.9% purity), 0.05 M methenamine ($C_6H_{12}N_4$, 99.9% purity), and 0%, 0.2%, 1%, and 2% gallium nitrate hydrate ($Ga(NO_3)_3{\cdot}xH_2O$, 99.9% purity). The substrates were placed downward in the above solutions at 90 °C for 2 h for the nanorods to grow. After the reaction, the substrates were removed from the solution, rinsed with deionized water thoroughly, and dried using nitrogen.

For making the nanorods with tip morphologies, nanorods were bound on a sputtering target by a carbon tape and exposed to oxygen plasma for 0, 30, 60, and 120 s. For the plasma treatment, process pressure and rf-power were maintained at 5×10^{-2} Torr and 30 W, respectively.

The morphology, size distribution, and crystal structure of all the nanorods were investigated by a field-emission scanning electron microscope (FE-SEM, Hitachi S-4700I), a transmission electron microscope (TEM, JEOL 2100F), and an X-ray diffractor (XRD, Bede D1). The chemical composition was estimated by an energy dispersive X-ray spectrometer (EDS, Oxford ISIS300). The field-emission current-voltage ($I-V$) curves of all nanorod emitters were measured at a pressure of 2×10^{-6} Torr kept by a turbo molecular pump. A copper tip was employed to act as an anode with a tip area of 7.09×10^{-3} cm^2 and p-type Si covered with ZnO emitters as a cathode with an area of 1 cm^2. We used micrometer (accuracy of ± 1 μm) to adjust the distance between the copper anode and nanorod emitters. The distances of the as-grown and other nanorod emitters with the anode are 100 and 150 μm, respectively. The field emission properties are affected by the anode area and anode–cathode distance based on the Filips model [19]. The turn-on and threshold fields are defined at current densities of 1 μA/cm^2 and 1 mA/cm^2, respectively. The dependence of the field emission current on the anode–cathode voltage was recorded using a programmable Keithley 237 picoammeter measurement system. The stability measurements were also carried out for the GZO nanorod emitters at temperatures of 25 °C, 50 °C, and 100 °C. The PL spectra were obtained using a He-Cd laser (325 nm) as an excitation source at room temperature.

III. Results and Discussion

Fig. 1(a)–(d) shows the FE-SEM morphologies of as-grown ZnO and Ga/Zn (GZO molar ratios of 0.2%, 1%, and 2% in solution) nanorod emitters. The as-grown nanorods vertically well-aligned over the ZnO seed layer/Si substrate have an average diameter of 200.7±21.4 nm and length of 1.79±0.11 μm. It can be observed that the small quantities of gallium doping would not significantly influence the length and diameter of the nanorod emitters. However, for the nanorod prepared with the solution of 2% Ga/Zn molar ratio, it shows very different morphology, and significant reduction

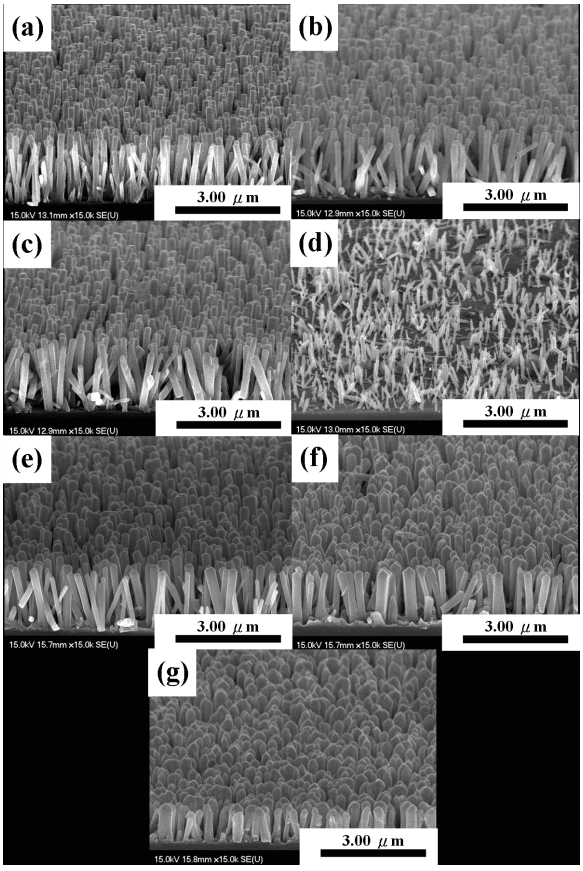

Fig. 1. Typical FE-SEM images of a ZnO nanorod with various Ga/Zn molar ratios in solution (a) 0% (as-grown), (b) 0.2%, (c) 1%, and (d) 2%, with various oxygen plasma treatment times, (e) 30 s, (f) 60 s, and (g) 120 s.

of number density, length, and diameter [Fig. 1(d)]. The higher amount of gallium doping has a great impact on the size, morphology, and number density of the nanorod emitters. The ZnO nanorods are formed by two different processes: nucleation and growth. The reactions can be explained as follows [20], [21]:

$$(CH_2)_6N_4 + 6H_2O \rightarrow 6HCHO + 4NH_3 \quad (1)$$

$$NH_3 + H_2O \rightarrow NH_4^+ + OH^- \quad (2)$$

$$4OH^- + Zn^{2+} \rightarrow Zn(OH)_4^{2-} \quad (3)$$

$$Zn(OH)_4^{2-} \rightarrow ZnO_{(s)} + H_2O + 2OH^-. \quad (4)$$

In our experiment, ZnO nanorod synthesis was performed in a closed system, that is, a limited amount of ZnO precursor in a specific period of time. As the Ga/Zn molar ratio at the solution is increased, the additional gallium ions prefer to react with the OH^- in the solution. This reaction reduces the ZnO content at the nucleation sites [22]. Therefore, the number density of ZnO nanorod arrays decreases as the gallium nitrate concentration increases.

Fig. 1(e)–(g) shows the FE-SEM morphologies of the oxygen plasma–treated (etching times of 30, 60, and 120 s) ZnO nanorod emitters. The morphology of ZnO nanorod emitters reveals dramatic change due to the oxygen plasma treatment. During the oxygen plasma treatment for 30 s, the top's structure of the nanorods is tower-shaped. By increasing the treatment time to 60 s, the tip structure of the ZnO

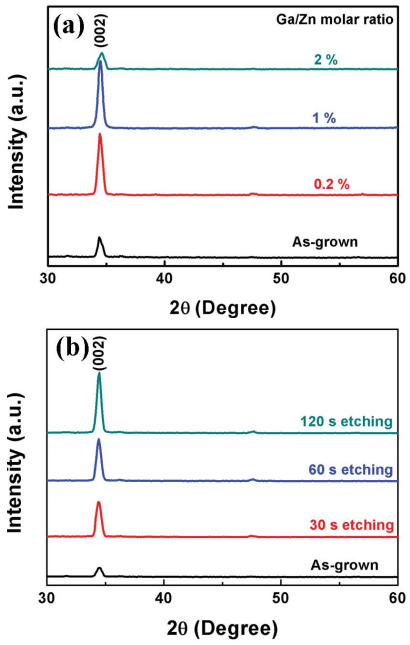

Fig. 2. XRD analysis of (a) GZO nanorod with various Ga/Zn molar ratios in solution. (b) ZnO nanorod emitters with the various oxygen plasma eching times.

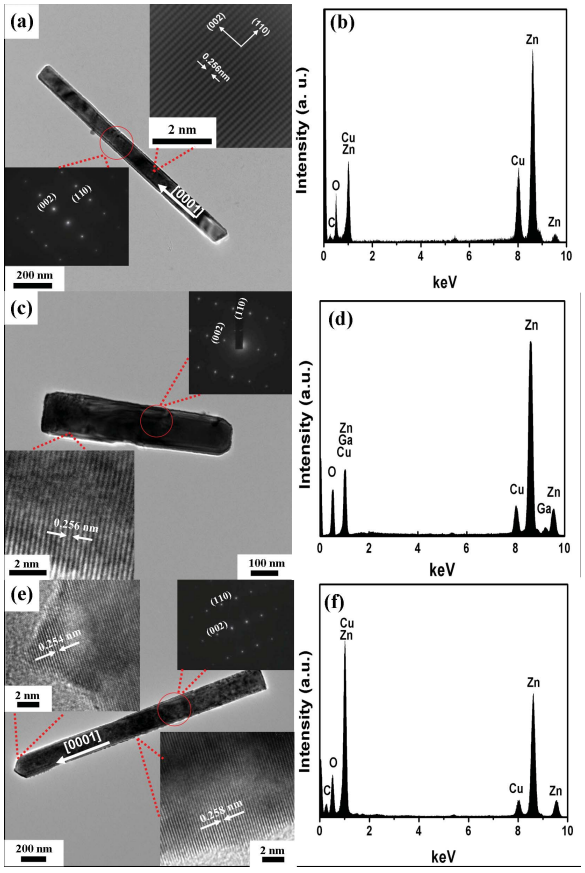

Fig. 3. TEM bright field image, corresponding to SAED pattern, HR-TEM image, and EDS analysis of different nanorods. (a) and (b) As-grown ZnO nanorod. (c) and (d) (GZO molar ratio of 2%) nanorod. (e) and (f) As-grown ZnO nanorod after oxygen plasma etching for 60 s.

nanorod emitters is formed. The formation of acute nanotips morphology is due to the oxygen ion bombardment at the edge of the nanorods leading to isotropic etching [18]. Fig. 1(g) shows the morphology of the nanorods plasma treated for 120 s, indicating a destruction due to over-etched and a decrease in aspect (c/a) ratio of the nanorods, which will degrade the performance of the emitters [23].

Fig. 2(a) and (b) shows the XRD spectra of the as-grown ZnO, GZO, and various oxygen plasma–etched ZnO nanorod emitters. It indicates that all the nanorods belong to the single phase hexagonal wurtzite structure with preferred (002) orientation. Fig. 2(a) depicts that the (002) peak shifts to high angle (from 34.3° to 34.6°), as Ga/Zn ratio changes from 0% to 2%, since the ionic radius of the gallium ion (0.62 Å) is smaller than that of the zinc ion (0.74 Å). However, the intensity of (002) peak of (GZO molar ratio of 2%) nanorods is reduced probably due to lattice distortion caused by the larger amount of gallium ions. Fig. 2(b) shows that the intensity of the (002) diffraction peak increases with an increase of the oxygen plasma bombardment time up to 120 s. It indicates that the bombardment of the oxygen ions not only helps to form the tip structure but also oxidizes the oxygen vacancies at the ZnO nanorods.

The crystalline properties and morphology of the nanorods have been studied using the plane view TEM observations. The bright field images, selected area electron diffraction (SAED) pattern, and EDS analysis of the as-grown ZnO, (GZO molar ratio of 2%), and as-grown ZnO nanorods after the oxygen plasma treatment for 60 s are shown in Fig. 3(a)–(f). The (002) c-axis interplanar spacing is 2.56 Å [insets in Fig. 3(a) and (c)], which is consistent with the XRD results. The SAED patterns [insets in Fig. 3(a) and (c)] observe that the preferred growth of the nanorod is in the [0001] direction. The typical EDS spectrum [Fig. 3(b)] indicates that the as-grown nanorods are composed of only Zn and O. No evidence of other impurities is found from the spectrum. With further quantitative analysis of EDS, it reveals that the atomic ratio of Zn/O is 49.13:50.87, which is close to the stoichiometric ratio. The EDS spectrum [Fig. 3(d)] for the GZO nanorods reveals that the atomic ratio of Ga/Zn is 1.73±0.11%. Table I lists the comparison between the Ga/Zn molar ratios in the solution and the measured Ga/Zn atomic ratio. It shows no significant differences between them, which confirms the successful doping of gallium ions into ZnO nanorods by the solution method. Fig. 3(e) shows that the nanorod has a small tip, which is consistent with the result of FE-SEM observation and the tip angle approximately 100° can be obtained. The SAED pattern [insets in Fig. 3(e)] shows the preferred [0001] growth of the ZnO nanorods. The high-resolution images shown in insets of Fig. 3(e) reveal that the tip and the side of the nanorods have lattice planes with interplanar spaces of 2.54 and 2.58 Å, respectively, indicating the ZnO nanorods are wurtzite structure with [0001] direction. It is also observed that the tip area is a smooth surface with no cracks, indicating that the oxygen plasma treatment is a fast and powerful nanoscale surface modification method. The EDS spectrum shown in Fig. 3(f) indicates that the constituent elements of the nanorod are only composed of Zn and O having atomic ratio of Zn/O as 48.7:51.3.

TABLE I
EXTRACTED DATA OF THE Ga/Zn ATOMIC RATIOS, CARRIER CONCENTRATION AND FIELD EMISSION PROPERTIES OF GZO NANOROD EMITTERS AT DIFFERENT Ga/Zn MOLAR RATIOS IN SOLUTION

Emitters	Ga/Zn molar ratio in solution (%)	Real Ga/Zn atomic ratio of GZO nanorod based on EDS analyzed results (%)	Carrier concentration (cm^{-3})	Turn-on field (V/μm)	Threshold field (V/μm)	β value
As-grown ZnO nanorod	0	0	2.13×10^{17}	6.25	10.00	741
GZO nanorod	0.2	0.16 ± 0.05	5.12×10^{17}	4.29	6.86	1133
	1	0.85 ± 0.06	5.89×10^{17}	2.67	3.87	1905
	2	1.73 ± 0.11	9.89×10^{17}	3.71	5.57	1321

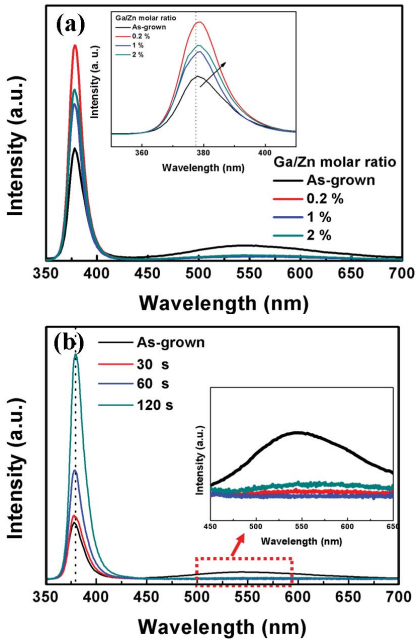

Fig. 4. Room temperature PL spectra of (a) GZO nanorod with various Ga/Zn molar ratios in solution (inset show magnify of UV emission areas) and (b) ZnO nanorod emitters with the various oxygen plasma etching times (inset show magnify of green emission areas).

The room-temperature PL spectra of the as-grown ZnO, GZO, and oxygen plasma–etched ZnO nanorod emitters are shown in Fig. 4(a) and (b). The strong ultraviolet (UV) emissions for those nanorods occur at about 378 nm, which comes from the recombination of exciton. The broad emission band is located at about 550 nm, which is the green emission of the visible spectrum. These peaks occur from the oxygen vacancies of the nanorods [24], [25]. The inset of Fig. 4(a) indicates that the peaks are red-shifted (from 377 to 379 nm) with an increase of gallium doping level. A similar red shift was also observed in Ga-, In-, and Sn-doped ZnO nanowires [14], [15]. The free electron density increases with an increase of gallium, resulting in renormalization of the band gap and thus leading to a red shift of the optical transitions. It is known that oxygen vacancies are the common defect in the n-type ZnO, which are relative to the visible emission. Fig. 4(a) and (b) indicates the intensity of the visible emission decreases, due to the decrease in oxygen vacancy concentration by gallium doping and oxygen plasma treatment. Previously, the reduced oxygen vacancy concentration of ZnO nanorods by annealing at various temperatures in an oxygen atmosphere was reported [26]. Thus, the reduced green emission is expected to occur by annealing at the oxygen atmosphere. Inset of Fig. 4(b) shows the decrease in green emission peak intensity, indicating clearly the decreased oxygen vacancy concentration and consequently the enhanced intensity of UV emission during oxygen plasma treatment occurred.

It was reported that the GZO nanorods provide much higher electron concentration with reduction of resistivity and lowers the voltage drop at the nanorod emitters [27]. On the other hand, the n-type doping can increase the possibility of electrons tunneling by lifting the Fermi level and reduce the work function of the nanorod emitters. We measured the carrier concentration of GZO nanorods (as listed in Table I) by the traditional Hall effect measurement. The relation between the electron concentration and the Fermi level can be written as follows [28]:

$$n = 2\left(\frac{2\pi m^* kT}{h^2}\right)^{1.5} \exp\left[-\frac{(E_c - E_f)}{KT}\right] \tag{5}$$

where n is carrier concentration, m^* the electron effective mass, k the Boltzmann constant, T the absolute temperature, h the Plank's constant, and E_f and E_c are energies at the Fermi level and bottom of conduction band, respectively. Using the carrier concentration (n), $m^* = 0.23m_0$ (m_0 is the electron static mass) and $q\chi = E_{\text{vacuum}} - E_C = 4.35$ eV for ZnO, the work functions ($\varphi = E_{\text{vacuum}} - E_f$) of the GZO nanorod emitters with 0.2%, 1%, and 2% of Ga/Zn molar ratios in the solution are estimated to be 4.65, 4.57, and 4.56 eV, respectively.

Fig. 5(a) and (c) shows the J–E curves of the as-grown ZnO, GZO, and oxygen plasma–etched ZnO nanorod emitters. The field emission current–voltage characteristics are analyzed by using the Fowler–Nordheim (F–N) equation [19], [29]

$$J = A\left(\frac{\beta^2 E^2}{\phi}\right)\exp\left(-\frac{B\phi^{1.5}}{\beta E}\right) \tag{6}$$

$$\ln\left(\frac{J}{E^2}\right) = \ln\left(\frac{A\beta^2}{\phi}\right) - \frac{B\phi^{1.5}}{\beta E} \tag{7}$$

where J is the current density, E the applied electric field, $A = 1.56 \times 10^{-10}$ (AeV/V^2), $B = 6.83 \times 10^9$ (V/eV$^{1.5}$m), β a field enhancement factor, and φ the work function of the emitter. When the work functions of the ZnO and GZO nanorods are known, the field enhancement factor can be

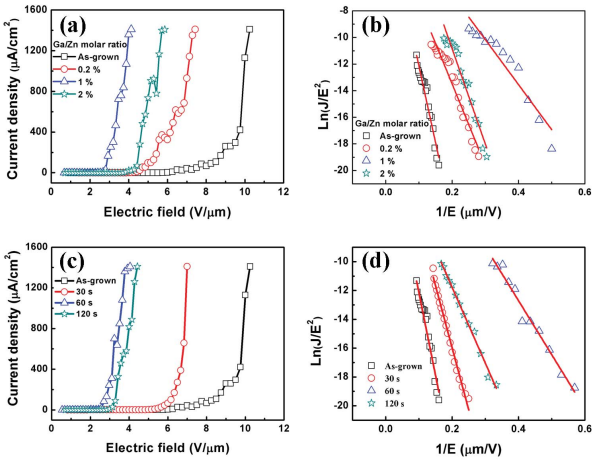

Fig. 5. (a) J–E curves and (b) F–N plots of GZO nanorod emitters with various Ga/Zn molar ratios in solution. (c) and (d) ZnO nanorod emitters with various oxygen plasma treatment times.

TABLE II
FIELD EMISSION PROPERTIES OF ZnO NANOROD EMITTERS WITH VARIOUS OXYGEN PLASMA ECHING TIMES

Emitters	Oxygen plasma bombardment time (sec)	Turn-on field (V/μm)	Threshold field (V/μm)	β value
ZnO nanorod	0	6.25	10.00	741
	30	5.17	6.83	1012
	60	2.43	3.61	2268
	120	3.00	4.14	1824

calculated from the slope of the F–N plots shown in Fig. 5(b) and (d). The field emission properties of the nanorods with various Ga/Zn molar ratios in the solutions and different oxygen plasma treatment times are listed in Tables I and II. With an increase of the Ga/Zn molar ratio in the solution, it also increases carrier concentration and reduces the turn-on field of the nanorod emitters. The GZO nanorods prepared with Ga/Zn of 1% in solution show optimum field emission properties among those nanorods. Its turn-on field, threshold field, and field enhancement factor are 2.67 V/μm, 3.87 V/μm, and 1905, respectively. On the other hand, the GZO nanorods prepared with the solution of 2% Ga/Zn molar ratio, it shows the significant reduction of length, diameter, and crystallization from the FE-SEM and XRD results, which will decrease the field emission properties of the nanorod emitters. Therefore, the measured field emission results confirm that the gallium doped into the ZnO nanorod emitters provides high carrier concentration and reduces the work function of the nanorod emitters, which exhibits lower turn-on field, threshold field, and larger field enhancement factor.

Regarding the oxygen plasma treatment, the ZnO nanorod with 60-s treatment shows the best field emission properties. The turn-on field, threshold field, and field enhancement factor are found to be 2.42 V/μm, 3.61 V/μm, and 2268, respectively. Based on Filips model, β is approximately equal to $(1 + s(d/r))$, where s is dependent on screen effect,

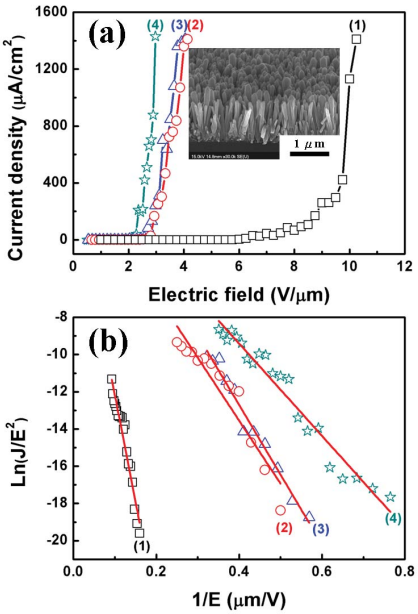

Fig. 6. (a) J–E curves and (b) F–N plots of nanorod emitters with different treated processes: 1) as-grown ZnO nanorod; 2) GZO nanorod (Ga/Zn molar ratio of 1% in solution); 3) as-grown ZnO nanorod with oxygen plasma etching for 60 s; and 4) GZO nanorod (Ga/Zn molar ratio of 1% in solution) with oxygen plasma etching for 60 s and the inset show the FE-SEM image of tip structure GZO nanorod emitters.

d the distance between the anode and the cathode, and r the radius of the emitters. In our experiment, the different etched time emitters are considered with the same nanorods number density of 18.5/μm^2 and from FE-SEM images and the same distance between tips and the anode plate. The aspect ratios (c/a) of ZnO nanorods with 30-s and 60-s oxygen plasma etching are estimated to be 6.74±0.99 and 5.41±1.10, respectively. Clearly, the nanorods with sharp tips have high β values. In our case, the optimum oxygen plasma–etched time for the nanorods is 60 s. These nanorod emitters show lower turn-on field, uniform morphology distribution, and high crystallinity. On the other hand, the ZnO nanorods with 120-s oxygen plasma treatment show decrease in aspect ratio (c/a) and destruction of nanorods from FE-SEM observation, which would degenerate the field emission properties.

Based on the above results, we realize that the GZO nanorods (Ga/Zn molar ratio of 1% in solution) with oxygen plasma treatment time for 60 s exhibit the optimum field emission properties. The FE-SEM images [inset in the Fig. 6(a)] shows the tip structure of these GZO nanorod emitters, indicating that the GZO nanorods can be easily sharpened and exhibit a tip angle approximately 100° by oxygen plasma treatment for 60 s.

The J–E curves and F–N plots of nanorod emitters with different etched times are shown in Fig. 6(a) and (b), respectively. The (GZO molar ratio of 1% in solution) nanorod emitters with tip angle of 100° have the best field emission properties among those emitters, with turn-on field of 1.99 V/cm, threshold field 2.91 V/cm, and field enhancement factor 2465. The comparison of field emission properties

TABLE III
FIELD EMISSION PROPERTIES OF NANOROD EMITTERS WITH VARIOUS TREATED PROCESSES

Emitters	Turn-on field (V/μm)	Threshold field (V/μm)	β value
As-grown ZnO nanorod	6.25	10.00	741
GZO nanorod (Ga/Zn molar ratio of 1% in solution)	2.67	3.87	1905
As-grown ZnO nanorod + oxygen plasma for 60 s	2.43	3.61	2268
GZO nanorod (Ga/Zn molar ratio of 1% in solution) + oxygen plasma for 60 s	1.99	2.91	2465

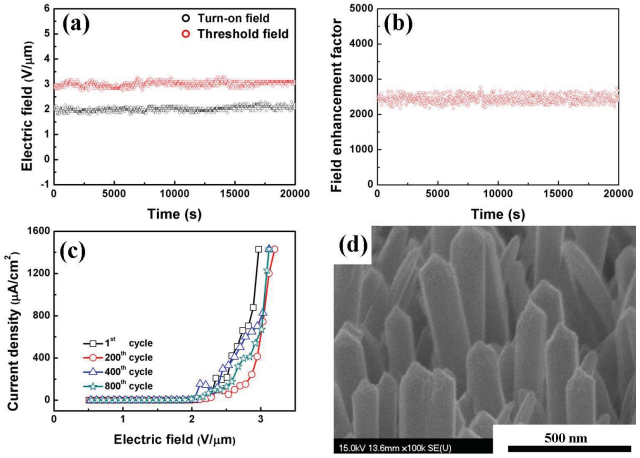

Fig. 7. Stability at 25 °C of GZO nanorod (Ga/Zn molar ratio of 1% in solution) with oxygen plasma etching for 60 s. (a) Turn-on and threshold fields. (b) Field-emission enhancement factor. (c) 1st, 200th, 400th, and 800th cycle respective J–E curves. (d) FE-SEM images of tip-structured GZO nanorod emitters for stability tests.

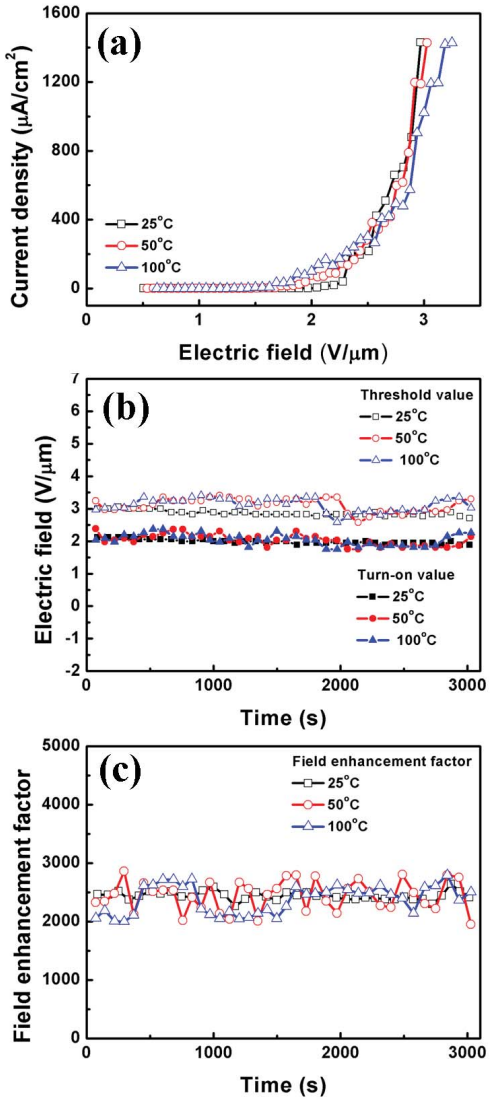

Fig. 8. Stability at various temperatures of tip structure GZO nanorod emitters. (a) J–E curves. (b) Turn-on and threshold fields. (c) Field-emission enhancement factor.

of nanorod emitters with different treatments are listed in Table III. The results demonstrate that combination of gallium doping and oxygen plasma treatment is able to successfully improve the field emission properties of the nanorod emitters, which not only reveal the low turn-on and threshold fields and high β value but also exhibit good stability. Fig. 7(a) and (b) depicts the stability characteristics of 2×10^4 s at 25 °C for the tip-structured GZO nanorod (Ga/Zn molar ratio of 1% in solution) emitters and shows the variations of turn-on field, threshold field, and field enhancement factor are 2.01±0.09 V/μm, 3.00±0.10 V/μm, and 2440.2±108.7, respectively. Fig. 7(c) depicts the J–E curves for 1st, 200th, 400th, and 800th operation cycles of these tip-structured GZO nanorod emitters. The stable and reproducible field emission properties can be observed for up to 800 cycling tests. After the stability tests, the morphology of nanorod emitters was observed using FE-SEM and it still exhibits the nanotips on the nanorod emitters [shown in Fig. 7(d)] and implies the tip-structured GZO nanorod emitters provide the enough lifetime and operation cycles for field emission device applications.

Fig. 8(a) depicts the J–E curves at temperatures 25 °C, 50 °C, and 100 °C for tip-structured (GZO molar ratio of 1% in solution) nanorod emitters. It is indicated that the nanorod emitters can be successively and stably operated between 25 °C and 100 °C. During the cycling test for 3000 s, the turn-on fields are 2.06±0.11, 2.08±0.13 and 2.07±0.13 V/μm; the threshold fields are 3.01±0.15, 3.07±0.16 and 3.09±0.17 V/μm; the field enhancement factor are 2442.3±97.1, 2416.0±131.0, and 2413.6±240.5 at the 25 °C, 50 °C, and 100 °C, respectively, which can be calculated according to the J–E curves as shown in Fig. 8(b) and (c). According to the crystal defect theory, the probability (ρ) of oxygen ions to overcome the potential barrier and create vacancies can be expressed as follows [30]:

$$\rho \approx \nu \exp\left(-\frac{E}{k_B T}\right) \tag{8}$$

where ν is a characteristic atomic vibrational frequency, E the potential barrier height, and T the temperature. Thus, with an increase of temperature, the probability of defect formation

is increased. However, in the present case, the nanorod emitters still exhibit the stable and reversible field emission properties at temperatures 25 °C–100 °C. Thus, oxygen plasma etching process has the advantage of obtaining more stable field emission characteristic up to 100 °C. This phenomenon may be attributed to decreasing the concentration of oxygen vacancies of the nanorods and obtaining a better crystallinity after the treatment.

IV. Conclusion

In summary, we successfully enhanced the performance of ZnO employing gallium doping process and oxygen plasma treatment. The synthesized process is simple, low cost, and enables large-scale production. The (002) orientation and tip-structured morphology of the nanorod emitters were proved by XRD pattern, FE-SEM, and TEM observations. The PL spectrum revealed that the green emission peak that occurred from oxygen vacancies after oxygen plasma treatment is lowered and obviously this phenomenon is due to the reduction in the concentration of oxygen vacancies of the nanorod emitters. The vertically aligned nanorod emitters reduced their work functions and increase their electron charge carrier concentration through gallium doping process. The tip-structured nanorod emitters can be formed after oxygen plasma treatment. Thus, in combining the gallium doping and the oxygen plasma treatment, the tip-structured GZO nanorod emitters have enhanced performance, including lower turn-on and threshold fields, higher field enhancement factor, and good stability characteristics over 2×10^4 s at room temperature. In addition, the tip-structured (GZO molar ratio of 1% in solution) nanorod emitters can successfully and stably operate up to 100° without notable degradation of emission properties. Therefore, these tip-structured ZnO nanorod emitters could be used in electron field emission and light emitting applications in the future.

References

[1] J. T. Hu, T. W. Odem, and C. M. Lieber, "Chemistry and physics in one dimension: Synthesis and properties of nanowires and nanotubes," *Accounts Chem. Res.*, vol. 32, no. 5, pp. 435–445, 1999.

[2] M. H. Huang, S. Mao, H. Feick, H. Yan, Y. Wu, H. Kind, E. Webber, R. Russo, and P. Yang, "Room-temperature ultraviolet nanowire nanolasers," *Science*, vol. 292, no. 5523, pp. 1897–1899, 2001.

[3] Z. H. Chen, Y. B. Tang, Y. Liu, G. D. Yuan, W. F. Zhang, J. A. Zapien, I. Bello, W. J. Zhang, C. S. Lee, and S. T. Lee, "ZnO nanowire arrays grown on Al:ZnO buffer layers and their enhanced electron field emission," *J. Appl. Phys.*, vol. 106, no. 6, pp. 064303-1–064303-6, 2009.

[4] C. C. Chuang, J. H. Huang, C. C. Lee, and Y. Y. Chang, "Fabrication and field emission characteristics of high density carbon nanotube microarrays," *J. Vac. Sci. Technol. B*, vol. 23, no. 2, pp. 772–775, 2005.

[5] W. J. Zhang, Y. Wu, C. Y. Chan, W. K. Wang, X. M. Meng, I. Bello, Y. Lifshitz, and S. T. Lee, "Structuring single- and nano-crystalline diamond cones," *Diamond Relat. Mater.*, vol. 13, nos. 4–8, pp. 1037–1043, 2004.

[6] C. Y. Lee, M. P. Lu, K. F. Liao, W. W. Wu, and L. J. Chen, "Vertically well-aligned epitaxial $Ni_{31}Si_{12}$ nanowire arrays with excellent field emission properties," *Appl. Phys. Lett.*, vol. 93, no. 11, pp. 113109-1–113109-3, 2008.

[7] C. Y. Lee, S. Y. Li, P. Lin, and T. Y. Tseng, "Field-emission triode of low-temperature synthesized ZnO nanowires," *IEEE Trans. Nanotechnol.*, vol. 5, no. 3, pp. 216–219, May 2006.

[8] C. Y. Lee, T. Y. Tseng, S. Y. Li, and P. Lin, " Electrical characterizations of a controllable field emission triode based on low temperature synthesized ZnO nanowires," *Nanotechnology*, vol. 17, no. 1, pp. 83–88, 2006.

[9] D. Banerjee, S. H. Jo, and Z. F. Ren, "Enhanced field emission of ZnO nanowires," *Adv. Mater.*, vol. 16, no. 22, pp. 2028–2032, 2004.

[10] Q. Wan, K. Yu, T. H. Wang, and C. L. Lin, "Low-field electron emission from tetrapod-like ZnO nanostructures synthesized by rapid evaporation," *Appl. Phys. Lett.*, vol. 83, no. 11, pp. 2253–2255, 2003.

[11] U. Ozgur, Y. I. Alivov, C. Liu, A. Teke, M. A. Reshchikov, S. Dogan, V. Avrutin, S. J. Cho, and H. Morkoc, "A comprehensive review of ZnO materials and devices," *J. Appl. Phys.*, vol. 98, no. 4, pp. 041301-1–041301-103, 2005.

[12] L. A. Xu, Y. Su, Y. Q. Chen, H. H. Xiao, L. A. Zhu, Q. T. Zhou, and S. Li, "Synthesis and characterization of indium-doped ZnO nanowires with periodical single-twin structures," *J. Phys. Chem. B*, vol. 110, no. 13, pp. 6637–6642, 2006.

[13] X. Y. Xue, L. M. Li, H. C. Yu, Y. G. Wang, and T. H. Wang, "Extremely stable field emission from AlZnO nanowire arrays," *Appl. Phys. Lett.*, vol. 89, no. 4, pp. 043118-1–043118-3, 2006.

[14] S. Y. Bae, C. W. Na, J. H. Kang, and J. Park, "Comparative structure and optical properties of Ga-, In-, and Sn-doped ZnO nanowires synthesized via thermal evaporation," *J. Phys. Chem. B*, vol. 109, no. 7, pp. 2526–2531, 2005.

[15] S. Y. Li, P. Lin, C. Y. Lee, T. Y. Tseng, and C. J. Huang, "Effect of Sn dopant on the properties of ZnO nanowires," *J. Phys. D, Appl. Phys.*, vol. 37, no. 16, pp. 2274–2282, 2004.

[16] J. Zhong, S. Muthukumar, Y. Chen, Y. Lu, H. M. Ng, W. Jiang, and E. L. Garfunkel, "Ga-doped ZnO single-crystal nanotips grown on fused silica by metalorganic chemical vapor deposition," *Appl. Phys. Lett.*, vol. 83, no. 16, pp. 3401–3403, 2003.

[17] C. Xu, M. Kim, J. Chun, and D. Kim, "Growth of Ga-doped ZnO nanowires by two-step vapor phase method," *Appl. Phys. Lett.*, vol. 86, no. 13, pp. 133107-1–133107-3, 2005.

[18] I. C. Yao, P. Lin, and T. Y. Tseng, "Nanotip fabrication of zinc oxide nanorods and their enhanced field emission properties," *Nanotechnology*, vol. 20, no. 12, p. 125202, Mar. 2009.

[19] V. Filip, D. Nicolaescu, M. Tanemura, and F. Okuyama, "Modeling the electron field emission from carbon nanotube films," *Ultramicroscopy*, vol. 89, nos. 1–3, pp. 39–49, 2001.

[20] Q. Li, V. Kumar, Y. Li, H. Zhang, J. T. Mark, and R. P. H. Chang, "Fabrication of ZnO nanorods and nanotubes in aqueous solutions," *Chem. Mater.*, vol. 17, no. 5, pp. 1001–1006, 2005.

[21] S. Ma, G. Fang, C. Li, S. Sheng, L. Fang, Q. Fu, and X. Zhao, "Controllable synthesis of vertically aligned ZnO nanorod arrays in aqueous solution," *J. Nanosci. Nanotechnol.*, vol. 6, no. 7, pp. 2062–2066, 2006.

[22] H. Wang, S. Baek, J. Song, J. Lee, and S. Lim, "Microstructural and optical characteristics of solution-grown Ga-doped ZnO nanorod arrays," *Nanotechnology*, vol. 19, no. 7, p. 075607, Feb. 2008.

[23] X. Qian, H. Liu, Y. Guo, Y. Song, and Y. Li, "Effect of aspect ratio on field emission properties of ZnO nanorod arrays," *Nanoscale Res. Lett.*, vol. 3, no. 8, pp. 303–307, 2008.

[24] K. Vanhausden, W. L. Warren, C. H. Seager, D. R. Tallant, J. A. Voigt, and B. E. Gnade, "Mechanisms behind green photoluminescence in ZnO phosphor powders," *J. Appl. Phys.*, vol. 79, no. 10, pp. 7983–7990, 1996.

[25] Y. P. Wang, W. I. Lee, and T. Y. Tseng, "Degradation phenomena of multilayer ZnO-glass varistors studied by deep level transient spectroscopy," *Appl. Phys. Lett.*, vol. 69, no. 12, pp. 1807–1809, 1996.

[26] S. N. Bai, H. H. Tsai, and T. Y. Tseng, "Structural and optical properties of Al-doped ZnO nanowires synthesized by hydrothermal method," *Thin Solid Films*, vol. 516, nos. 2–4, pp. 155–158, 2007.

[27] C. X. Xu, X. W. Sun, and B. J. Chen, "Field emission from gallium-doped zinc oxide nanofiber array," *Appl. Phys. Lett.*, vol. 84, no. 9, pp. 1540–1542, 2004.

[28] S. M. Sze, *Physics of Semiconductor Devices*, 2nd ed. Singapore: Wiley, 1981, p. 17.

[29] F. M. Charbonnier, W. A. Mackie, R. L. Hartman, and T. B. Xie, "Robust high current field emitter tips and arrays for vacuum microelectronics devices," *J. Vac. Sci. Technol. B*, vol. 19, no. 3, pp. 1064–1073, 2001.

[30] C. Kittel, *Introduction to Solid State Physics*, 8th ed. Hoboken, NJ: Wiley, 2004, p. 590.

I-Chuan Yao was born in Changhua, Taiwan, in 1983. He received the B.S. degree from the Department of Materials Science and Engineering, National Formosa University, Yunlin, Taiwan, and the M.S. degree from the Institute of Materials Engineering, National Taipei University of Technology, Taipei, Taiwan, in 2005 and 2007, respectively. He is currently pursuing the Ph.D. degree with the Institute of Materials Science and Engineering, National Chiao Tung University, Hsinchu, Taiwan.

His current research interests include ZnO nanostructure, field emission display, and sensor devices.

Pang Lin received the Ph.D. degree from the Department of Materials Science and Engineering, University of California, Los Angeles, in 1984.

He is a Professor with the Department of Materials Science and Engineering, National Chiao Tung University, Hsinchu, Taiwan. His current research interests include semiconducting zinc oxide and energy materials.

Sheng-He Huang was born in Taichung, Taiwan, in 1987. He received the B.S. degree from the Department of Electrical Engineering, National Sun Yat Sen University, Kaohsiung, Taiwan, and the M.S. degree from the Department of Electronic Engineering, National Chiao Tung University, Hsinchu, Taiwan, in 2009 and 2011, respectively.

His current research interests include ZnO nanostructure and field emission display.

Tseung-Yuen Tseng (F'02) received the Ph.D. degree in electroceramics from the School of Materials Engineering, Purdue University, West Lafayette, in 1982.

He was briefly associated with the University of Florida, Gainesville, before joining National Chiao-Tung University, Hsinchu, Taiwan, in 1983, where he is currently a University Chair Professor with the Department of Electronics Engineering and the Institute of Electronics. He was the Dean of College of Engineering from 2005 to 2007, and the Vice Chancellor and University Chair Professor with the National Taipei University of Technology, Taipei, Taiwan, from 2007 to 2009. He is the Editor of the *Handbook of Nanoceramics and Their Based Nanodevices* (5-vol. set) and *Nonvolatile Memories: Materials, Devices, and Applications* (2-vol. set), Guest Editor of a special issue of Ferroelectrics (six volumes), and an Associate Editor of the *Journal of Nanoscience and Nanotechnology* and the *Advanced Science Letters and International Journal of Applied Ceramic Technology*. He has published over 290 research papers in refereed international journals and 110 conference papers, several book chapters, and holds 28 patents. His current research interests include electronic ceramics, nanoceramics, ceramic sensors, high-k dielectric films, ferroelectric thin films and their based devices, and resistive switching memory devices.

Dr. Tseng invented the base metal multilayer ceramic capacitors, which have become a large-scale commercial product. He is a Board Member of Asia Ferroelectrics Association and the General Chair of the sixth Asian Meeting of Ferroelectrics. He is a Chairperson, Session Chair, Keynote and Invited Speaker, and Member of Advisory Committee of many national and international meetings. He has received the Distinguished Research Award from the National Science Council from 1995 to 2001, the Hou Chin-Tui Distinguished Honor Award in 2002, Dr. Sun Yat-Sen Academic Award in 2003, the TECO Technology Award in 2004, the IEEE CPMT Exceptional Technical Achievement Award in 2005, the Distinguished Research Award of Pan Wen Yuan Foundation in 2006, the Academic Award of Ministry of Education in 2006, the Medal of Chih-Hung Lu in 2010, and the National Endowed Chair Professor in 2011. He was elected a fellow of the American Ceramic Society in 1998 and MRS-T Fellow in 2009.